Communication-System Blackout During Reentry of Large Vehicles

IBM No 67-U60-0025

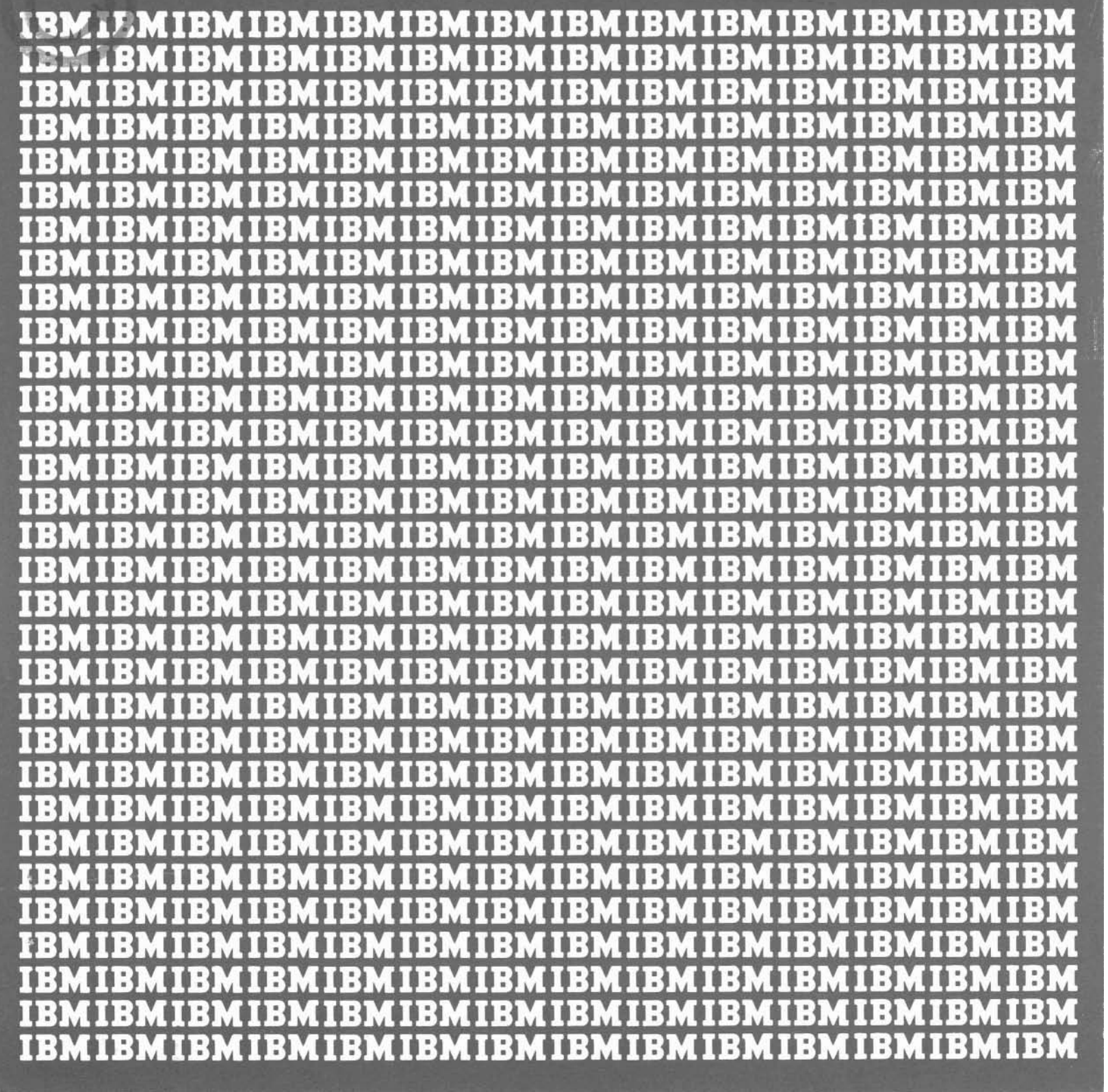

IBM No. 67-U60-0025
July 28, 1967

COMMUNICATION-SYSTEM BLACKOUT DURING REENTRY OF LARGE VEHICLES

by

Dr. F. H. Mitchell, Jr.

This paper was published in the
Proceedings of the IEEE
Volume 55, Number 5, May 1967.

Communication-System Blackout During Reentry of Large Vehicles

F. H. MITCHELL, JR., MEMBER, IEEE

Abstract—**Much of the theoretical research on reentry blackout is in a format difficult for the communications design engineer to use in his system analysis. This paper derives simplified equations for the average sheath power loss that may be added (in dB) to the usual space loss to obtain an approximate total propagation loss. The plasma and sheath properties are discussed in detail but largely without supporting mathematics, in order to give the design engineer a better understanding of the overall problem. For the same reason and to provide insight into the final results, the average radiated power is found, using both intuitive and rigorous techniques. Several graphs of plasma properties are included in the development as an aid to numerical computations, and results are compared with the work of other authors.**

I. Introduction

WHEN A MISSILE reenters the Earth's atmosphere with orbital velocity, a plasma sheath forms on its surface, and normal communications systems and transponder tracking systems are blacked out. As part of the vehicle communication-system design, the engineer needs to calculate the power sheath loss at various points during the reentry in order to predict the extent of the radio blackout. The following development is oriented toward such a design task. Interpolation between a few calculated radiation patterns can be used to obtain approximate antenna loss estimates. However, the value of this technique is reduced by the fact that nonlinear interpolation is required between patterns that have strong angular properties (Fig. 1) [1]. The communications design engineer needs a set of simplified equations and graphs to aid him in his system analysis. In deriving these aids, considerable justification exists for *smoothing out* some of the fine features of the theoretical antenna patterns since the geometric and electromagnetic assumptions made in their derivation cause one to doubt the reality of these features. One useful system property that fulfills the above requirement is the total power radiated through the sheath, and the following analysis is built around this variable.

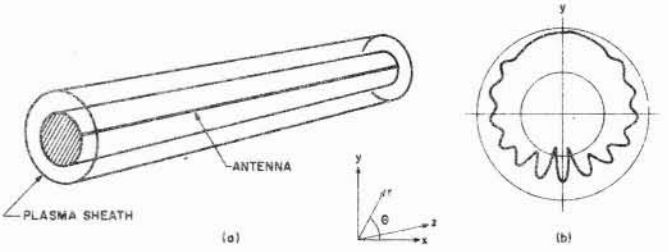

Fig. 1. Section of a conducting cylinder with an axial antenna. (a) Cylinder geometry. The cylinder has a normalized radius $k_0 a >> 1$, and it is assumed to be infinitely long. The radiated fields are independent of z. (b) Typical antenna pattern.

The antenna Q is described using a technique developed by Collin and Rothschild [2] to show how the radiated power is distributed among the different angular modes.

Communications power requirements without the plasma sheath can be found using standard techniques [3], and the plasma may be treated as an additional *space loss*. The plasma attenuation can be directly added (in dB) to the free-space system attenuation to obtain the total communications power loss. The low- and high-frequency properties of the plasma are described in order to place the various approximations in context and to point out their limitations. The studies of McCabe and Stolwyk [24], Hermann [25],

The author is with the Instrumentation and Communications Group of IBM Corporation, Federal Systems Division, Huntsville, Ala.

The plasma is formed behind a shock front that separates it from the normal atmosphere. The conservation of mass, momentum, and energy equations connect across the normal shock boundary and, when taken with the chemical rate equations, they theoretically enable one to compile a set of differential and algebraic equations to be solved for the abolute species concentrations and the collision rates between species behind the normal shock [9], [10]. However, the rate coefficients for the various plasma reactions are not known with any precision; the boundary conditions can only be applied in idealized form; and the numerical analysis is complex. For these reasons, only approximate calculations are possible. Figure 3 shows resultant electron densities and electron collision frequencies [25]. This data calculated for the point behind the normal shock may be extended to other positions on the missile surface [4], [6], [8], [18], [23], [24], [25]. These studies suggest that at a stream-line distance of $3a$ behind the normal shock, the drop in electron density is of the magnitude 10^{-2} [4], [6], [8], [23], after which the drop factor is 10^{-1} per $10a$ [24]. The collision frequency drops to about 10^{-1} of its normal shock value at $3a$ and continues to decrease in a ratio of 10^{-1} per $10a$. The plasma thickness above the antenna is often taken to be of the magnitude $0.5a$ [18], [25].

IV. The Langevin Equation

At sufficiently low frequencies, the plasma behaves like a conductor because of free electron and ion current carriers. The conductivity depends on the number of carriers, types of collisions, and other loss processes and is a function of the plasma temperature. Only the current contribution from the free electrons is considered here since, for a given applied force, the ion acceleration will be less than the electron acceleration by the ratio $m_e/m_i < 1/1800$.

The electron motion in a plasma is governed by the Lorentz equation

$$m\frac{d\bar{v}}{dt} = -|e|\bar{E} - |e|\bar{v}\times\bar{B} - mg\bar{v} \tag{2}$$

where $\bar{E}$ and $\bar{B}$ are the applied electric and magnetic fields, g is the collision frequency for momentum transfer between electrons and atoms or ions, and a term multiplied by the pressure gradient has been assumed negligible.

It may be shown from (2) that a plasma has an equivalent permittivity

$$\varepsilon = \varepsilon_0\left[1 - \frac{\omega_p^2}{\omega^2 + g^2} - \frac{i\omega_p^2 g}{\omega(\omega^2 + g^2)}\right] \tag{3}$$

where $\omega_p = \sqrt{N_e e^2/m\varepsilon_0}$ is the plasma frequency. For most reentry plasmas $\omega_p > g$.

The normalized complex propagation constant k_r is related to the index of refraction n and the absorption coefficient α by the equation

$$k_r^2 = \left(\frac{k}{k_0}\right)^2 = \varepsilon/\varepsilon_0 = (n + i\alpha)^2. \tag{4}$$

The plasma properties n and α are plotted as a function of ω/ω_p and g/ω_p in Figs. 4 and 5, and the following three regions can be noted:

$\omega < \omega_p$—absorption and dispersion high, typical of a metal,
$\omega \gtrsim \omega_p$—absorption low and n varying rapidly,
$\omega >> \omega_p$—plasma approximately transparent.

The plasma behaves much like a high-pass filter over the frequency range being considered. This description of the plasma is based solely on its conduction properties, which are generally dominant for $\omega \lesssim \omega_p$. However, when $\omega >> \omega_p$, the dipole polarization of the plasma will give rise to absorption lines and these terms must be included in ε.

V. Absorption Lines

The conductivity of plasma is due to the existence of free electrons and ions that have been formed by the intense heat. This heat will also raise some of the electrons into excited atomic and molecular states without completely freeing them. Since these electrons are weakly bound, the excited system is easily polarized by the electric field of the incident wave, and thus it will exhibit a large dipole moment [11]. The dipole polarization contribution to ε can be expressed through the susceptibility χ or polarization $\bar{P}$:

$$\bar{D} = \varepsilon\bar{E} = \varepsilon_0(1 + \chi)\bar{E} = \varepsilon_0\bar{E} + \bar{P}. \tag{5}$$

The degree of atomic or molecular electron-cloud distortion due to the applied electric field depends on the frequency of the field, since there are resonances every time $\omega = \mathcal{W}/h$, where $\mathcal{W}$ is the energy of available transitions.

The plasma behaves like a gas of damped oscillators with resonant frequencies $\omega_{01}, \omega_{02}, \cdots, \omega_{0s}, \cdots$

$$X = \sum_s \frac{\omega_s^2}{\omega_{0s}^2 - \omega^2 + i\omega g_s} \tag{6}$$

where

$$\omega_s = \sqrt{\frac{N_s e^2}{m_s \varepsilon_0}} \tag{7}$$

determines the maximum absorption and $\Delta_s = \omega_s^2/\omega_{0s}^2$ the resultant change in n through a given resonance. At very high frequencies (above the X-ray region) $k/k_0 = 1$, so that as ω decreases, n is increased above unity by the sum of the resonance changes $\sum_s \Delta_s$ passed in going to the lower frequency. A complete plasma spectrum is shown schematically in Fig. 6. It may be noted that the absorption lines are similar to a collection of series RLC circuits whose admittances Y_s peak at frequencies ω_{0s}.

Some calculations of the polarizability of excited states of atomic oxygen and nitrogen are presented along with estimates of the molecular contributions in Garrett and Mitchell [11]. The problem of completely specifying the magnitude of all sheath resonances is complicated by the variety of constituents, including products of heat-shield ablation.

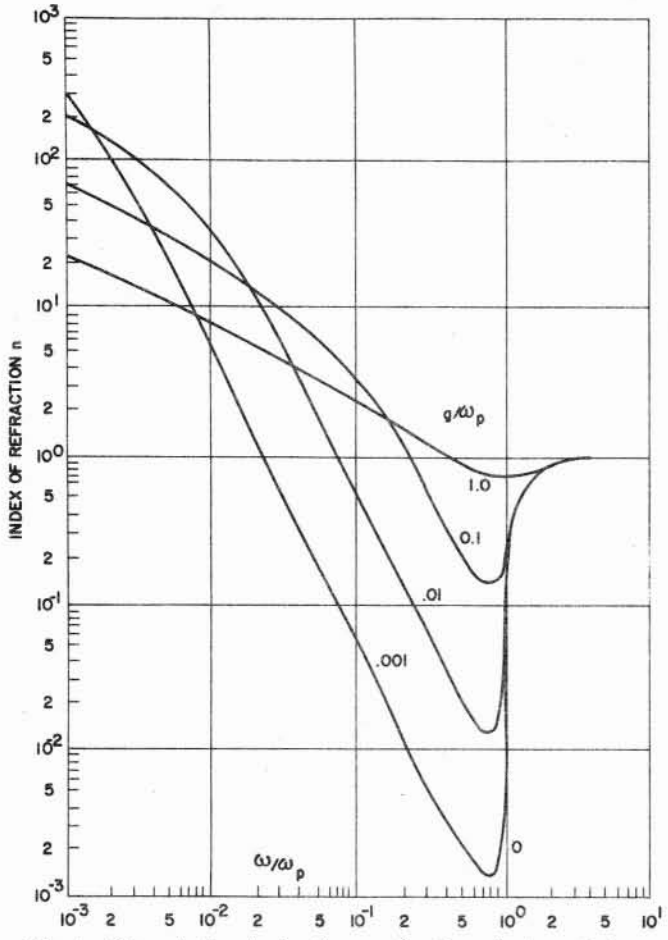

Fig. 4. Plasma index of refraction as a function of ω/ω_p and g/ω_p.

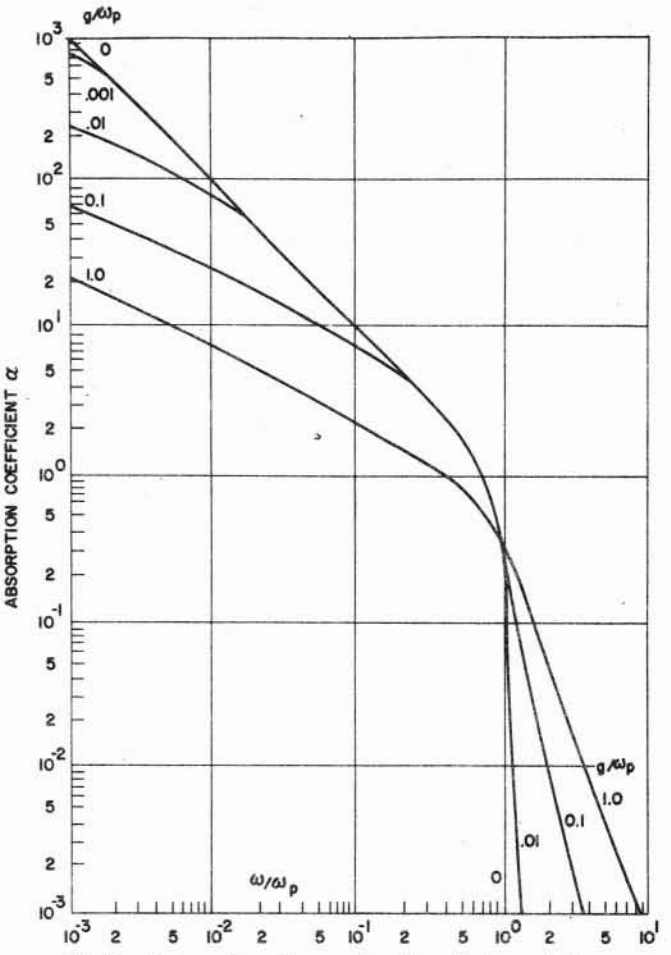

Fig. 5. Plasma absorption as a function of ω/ω_p and g/ω_p.

VI. Sheath Properties

The permittivity $\varepsilon(\omega_p, g)$ specifies the plasma properties for frequencies up through the microwave region and $\varepsilon(\omega_s, \omega_{0s}, g_s; s=1, 2, 3, \cdots)$ specifies the plasma properties within the resonance absorption region. In a real plasma sheath, ε is a complicated function of the physical variables that describe the plasma, including:

A. Constituents: The sheath will include free electrons, atoms and molecules of oxygen, nitrogen and argon, and ablation products. The simplest treatment at low frequencies is to consider only the free electron current. There is no simple treatment for the resonance absorption region [9], [10].

B. Time Dependence: The sheath properties vary with time during reentry. The adiabatic approximation assumes the sheath properties vary slowly with time when compared with the time required for transmission of a message [12].

C. Inhomogeneous Variations: The plasma properties will vary from place to place in the sheath. The first-order approximation here is to replace the actual varying ε by a constant, average ε_{AV} that has a step function transition at the edge of the plasma [13].

D. Nonlinear Effects: If the radiated fields are sufficiently strong, ε will be a function of the field intensity, requiring solution of a nonlinear differential equation [14].

E. Compression: The radiated fields can apply a force on the sheath and dissipate some energy in this way [15].

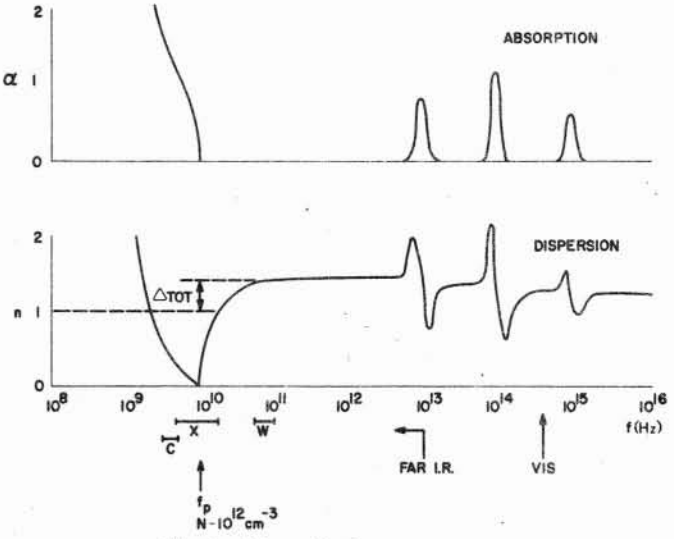

Fig. 6. Schematic plasma spectrum.

F. Plasma Waves: Longitudinal waves can exist in the plasma because of ion interactions, and these waves can affect the radiated fields [16].

G. Anisotropic Effects: The permittivity ε may become

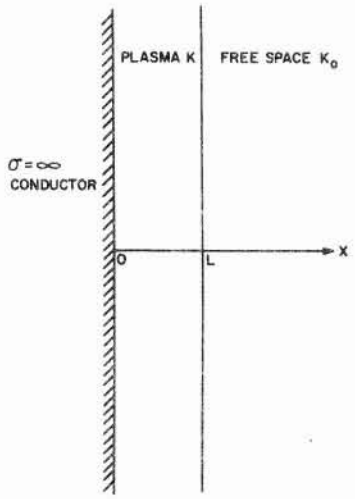

Fig. 7. A plane sheath adjoining a conductor.

a tensor if a magnetic field is applied to the plasma, giving different propagation properties in different directions [17].

A real plasma sheath is obviously not amenable to exact analytic studies. The usual approach taken is to consider only one or two of these complications in any given analysis and to neglect all the others. Care must be taken, of course, in the interpretation of any analysis carried out with these restrictions.

VII. The Simplest Model

Even the simplest sheath model provides useful insight into the interaction between the sheath and the radiated fields. This model is obtained by allowing the approximations discussed in Section VI-A through C and neglecting effects due to D through G. The sheath, missile, and antenna geometries are the same as those specified in Section I: a constant-phase magnetic line source on the surface of a perfectly conducting cylinder. Most manned vehicles of interest today have a normalized radius $k_0a \gg 1$ even at VHF frequencies (for example, the Saturn SIVB stage has a radius $a \approx 3.2$ m), and the model is based on this knowledge.

VIII. Plasma Sheath Attenuation

Before approaching the problem rigorously, an intuitive approach has been developed. The results of this method are shown in agreement with more strenuous calculations.

The loss in radiated power is a function of the plasma index of refraction n, absorption coefficient α and thickness k_0T, and the cylinder radius k_0a. The actual fields are a superposition of plane waves traveling in different directions with different propagation constants, and many essential features of the problem can be discussed by examining a single plane wave propagating in the x direction (Fig. 7). The wave is assumed set up by a radiating plane at $x=0$; waves partially reflected from $x=L$ and reincident on $x=0$ are totally reflected at this boundary because of the metal surface. A further approximation is to consider the loss effects to be due to a product of reflection and absorption losses.

From Part A of the Appendix, the total attenuation produced by the sheath is

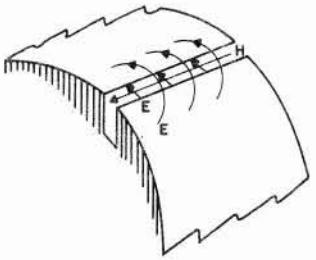

Fig. 8. Constant-phase magnetic line source on the surface of a cylinder.

$$\mathrm{dB} = -20\alpha k_0 L(\log e) + 10 \log\left(\frac{|1-R|^2}{|1-Re^{i\phi}|^2}\right) \tag{8}$$

where

$$R = (k_r - 1)/(k_r + 1). \tag{9}$$

If R is written in polar form $R_0 e^{i\theta_0}$, (8) becomes

$$\mathrm{dB} = -20\alpha k_0 L(\log e) + 10 \log\left(\frac{1-2R_0\cos\theta_0 + R_0^2}{1-2R_0e^{-\alpha k_0 L}\cos(\theta_0+nT)+R_0^2e^{-2\alpha k_0 L}}\right) \tag{10}$$

which is the desired final result. This equation can be used to find the sheath power loss, where $k/k_0 = n + i\alpha$ and $R_0e^{i\theta_0} = (k_r-1)/(k_r+1)$ can be found from Figs. 4 and 5.

Since the above analysis is for plane waves, it must be considered an average description of the processes taking place in the plasma and, when the attenuation predicted by the above equations is compared with more exact calculations, the latter, θ-dependent antenna patterns must be averaged over 2π to obtain the average attenuation factor.

The above results may also be obtained using a more rigorous approach. The radiated magnetic field from a plasma-clad constant-phase magnetic line source on the surface of a perfectly conducting cylinder (Fig. 8) is:

$$H_z = \frac{iE_0}{Z_0} \sum_{m=-\infty}^{+\infty} F_m H_m^{(1)}(k_0 r) e^{im\theta} \tag{11}$$

where the exciting field is a delta function

$$E_\theta(r = a) = E_0 \sum_{m=-\infty}^{+\infty} e^{im\theta}$$

From Part B of the Appendix, the radiated power is

$$P \approx \frac{E_0^2}{Z_0} \frac{(k_0a)^2 e^{-2\alpha k_0(r_1-a)}}{\left|1 + \frac{1}{2}\left(\frac{k}{k_0} - 1\right)(e^{2ik(r_1-a)}+1)\right|^2} \tag{12}$$

where r_1 is the outer radius of the plasma. If $\alpha = 0$, $n = 1$, the plasma vanishes and

$$P_0 \approx \frac{E_0^2}{Z_0}(k_0 a)^2. \tag{13}$$

The dependence of P_0 on $(k_0a)^2$ confirms that the network Q decreases for larger k_0a and is in agreement with more exact calculations [18]. Using the definitions of R from (9),

$$P = P_0 e^{-2\alpha k_0 L}\left(\frac{|1-R|^2}{|1-Re^{i\phi}|^2}\right) \tag{14}$$

as before in the intuitive treatment.

IX. Inhomogeneous Sheaths

For $\omega > \omega_p$, n is greater than α and may be slightly less than 1. Therefore,

$$\frac{P}{P_0} \propto [1-(1-n)(1-\cos\phi)][1-2\alpha T] \quad \omega > \omega_p. \tag{15}$$

This result is in agreement with other work [20], [21] by noting that

$$\frac{\varepsilon}{\varepsilon_0} \equiv 1 + \Delta = \frac{k^2}{k_0^2} \approx 1 + 2(1-n) \tag{16}$$

and

$$\text{field attenuation} = \tfrac{1}{2}\,(\text{power attenuation}). \tag{17}$$

For inhomogeneous sheaths, the ϕ-dependent form should be replaced by [20]

$$\tfrac{1}{2}[1-\cos\phi] \rightarrow \left[\frac{\phi}{1+\phi}\right] \tag{18}$$

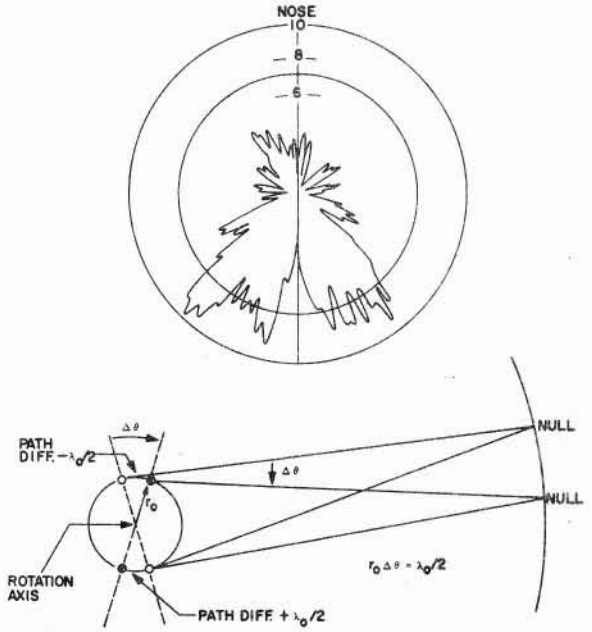

Fig. 9. Interference between dual VHF antennas, showing angular null separation $\Delta\theta = \lambda_0/2r_0$ [22].

to eliminate the artificial resonant-cavity properties of the step function solution.

X. Dual Antennas

Since $k_0a \gg 1$ for most missiles of interest today, the radiation patterns are fairly restricted to a half plane. Dual antennas have been introduced to obtain uniform coverage about the axis, and since k_0a is large, the interactions between the two antennas can be treated as perturbations on the individual radiation patterns. In-phase dual element systems are characterized by narrow interference nulls of angular period $\Delta\theta(\text{rad}) \approx \lambda_0/2a$ (Fig. 9) superimposed on the combined antenna patterns. The period ranges from 11° at 250 MHz (VHF) to 0.5° at 5.5 GHz (*C*-Band) [22], and a period of 0.08° would be expected with a millimeter system at 35 GHz (mm range). The change in radiated power due to these nulls is small, of the order $P/2k_0a$:

$$\begin{aligned}\Delta P &= \frac{E_0^2}{Z_{0\pi}}\frac{1}{2\pi}\int_0^{2\pi}\sum_{m,n=-\infty}^{+\infty} e^{im\theta}\, e^{-in(\theta+\pi)} F_m F_n^* \\ &= \frac{E_0^2}{Z_{0\pi}}\sum_{m=-\infty}^{+\infty}|F_m|^2(-1)^m \\ &= P_0\,\frac{\sum_{m=-k_0a}^{+k_0a}(-1)^m}{\sum_{m=-k_0a}^{+k_0a}(1)} \approx \frac{P_0}{2k_0a}.\end{aligned} \tag{19}$$

XI. Conclusions

A simple method for computing the average sheath power loss in dB has been found using both intuitive and rigorous approaches. The plasma properties n and α are graphed as functions of ω/ω_p and g/ω_p to facilitate the calculations for a given communications system of interest to the design engineer, and the basic properties of the plasma sheath have been described to aid in a general understanding of the approximations that have been used.

The blackout bounds for typical Apollo reentry trajectories can be found as an example of the above technique. Choose $g/\omega_p = 0$ and let a -20 dB drop in power define the beginning of cutoff. Only the absorption loss $= -8.68\alpha k_0 L$ (10) will be considered so that

$$\alpha_c k_0 L_c = 2.3 \tag{20}$$

defines the cutoff frequency. Assume $L_c \approx (2\pi/\lambda_0)\times(0.5a) = 0.06 f_c$ (MHz) so that $\alpha_c f_c$ (MHz) ≈ 40. In terms of the plasma frequency ω_p' above the antenna ($\approx 10^{-2}\,\omega_p$ behind the normal shock),

$$\alpha_c(100\omega_c/\omega_p) \approx \frac{40}{f_c(\text{MHz})}. \tag{21}$$

Now choose $f_c(\text{MHz}) = 250$ for the antenna frequency and from Fig. 4 find the value of ω/ω_p for which $\alpha_c \approx 0.16$:

$$100\,\frac{(2\pi \times 250)}{\omega_p(\text{MHz})} = 1.0 \tag{22}$$

$$\omega_p(\text{MHz}) = 15.7 \times 10^4 = 5.65 \times 10^{-2}\sqrt{N_e(\text{cm}^{-3})} \quad (23)$$

$$N_e \approx 8 \times 10^{12}/\text{cm}^3. \quad (24)$$

From Fig. 2 the blackout is seen to start at about 110 km at a vehicle speed of 11 km/s and end at 40 km at a vehicle speed of 4 km/s. This result compares favorably with computations by Lehnert and Rosenbaum [6] and Huber and Sims [8]. If the reflection loss were considered, the total loss would be $(-20\text{ dB})+(-8.5\text{ dB})=-28.5$ dB at 250 MHz so this term should not be considered negligible.

Hodara and Cohn [17] have predicted an absorption loss of -150 dB for $k_0L=1$, $\omega/\omega_p=0.05$, $g/\omega_p=0$, using asymptotic expansions for the case $k_0a\to\infty$. From Fig. 4, $k/k_0=i\,19$ so that an absorption loss of -166 dB is predicted from (10).

Appendix

Derivation of Plasma Attenuation

A. Plane Wave Approach

From the assumptions in Section VIII

$$P_{\text{rad}}/P_0 \propto f_{\text{abs}} \times f_{\text{refl}}. \quad (25)$$

Inside the plasma

$$\bar{H} = \bar{H}_0 e^{i(n+i\alpha)k_0x} \qquad \bar{E} = \frac{\bar{H}_0(n+i\alpha)e^{i(n+i\alpha)k_0x}}{\omega\varepsilon} \quad (26)$$

$$\bar{P} = \tfrac{1}{2}\,\text{Re}\,\bar{E}\times\bar{H}^* = \bar{x}\tfrac{1}{2}|H_0|^2 e^{-2\alpha k_0x}\,\text{Re}\,[Z_{\text{complex}}] \quad (27)$$

so that $f_{\text{abs}}\propto e^{-2\alpha k_0x}$.

To evaluate f_{refl}, consider the plasma to be a lossy medium with propagation constant k. Let a wave radiated from the plane $x=0$ be incident on the boundary $x=L$ so that

$$\bar{H}_{\text{inc}} = \bar{H}_0 e^{ik(x-L)} \qquad \bar{H}_{\text{refl}} = R\bar{H}_0 e^{-ik(x-L)} \quad (28)$$

$$\bar{H}_{\text{trans}} = T\bar{H}e^{ik_0(x-L)} \quad (29)$$

where R and T are the reflection and transmission coefficients.

By requiring $\bar{E}$ and $\bar{H}$ to be continuous

$$T = 2/(k_r+1)$$
$$R = (k_r-1)/(k_r+1) \quad (30)$$

with $k_r=n+i\alpha$ defined in Figs. 4 and 5 as a function of ω/ω_p and g/ω_p. The reflected wave will then propagate back to the plane $x=0$ and be totally re-reflected toward $x=L$. This process will continue so that

$$T_{\text{total}} = T + RTe^{i\phi} + R^2Te^{2i\phi} + \cdots \quad (31)$$

where $\phi=2kT$ is the phase shift undergone by the wave during each reflection. The two phase changes of π each at the boundaries, cause a total change of 2π and can be neglected. Therefore,

$$T_{\text{total}} = T[1 + (Re^{i\phi}) + (R^2e^{2i\phi}) + \cdots] \quad (32)$$

$$T_{\text{total}} = \frac{T}{1-Re^{i\phi}}.$$

For the reflection loss

$$f_{\text{refl}} \propto |T_{\text{total}}|^2 = \frac{|T|^2}{|1-Re^{i\phi}|^2}. \quad (33)$$

Within the framework of the model that has been chosen

$$P_{\text{rad}}/P_0 \propto \frac{|T|^2}{|1-Re^{i\phi}|^2}\,e^{-2\alpha k_0L} \quad (34)$$

and the total attenuation in dB is

$$\text{dB} = -20k_0L(\log e) + 10\log\left(\frac{|1-R|^2}{|1-Re^{i\phi}|^2}\right). \quad (35)$$

B. Large Cylinder Approach

From (11) and (12) and the boundary conditions at the outer plasma radius r_1

$$F_m = H_m^{(1)}(kr_1)/H_m'^{(1)}(ka)H_m^{(1)}(k_0r_1) \times \left\{1 + \frac{\pi kr_1}{2}\left[\frac{k}{k_0}\frac{H_m'^{(1)}(k_0r_1)}{H_m^{(1)}(k_0r_1)} - \frac{H_m'^{(1)}(kr_1)}{H_m^{(1)}(kr_1)}\right]\left[\frac{H_m^{(1)}(kr_1)}{H_m^{(1)}(ka)}\right] \times [J_m(kr_1)Y_m'(ka) - Y_m(kr_1)J_m'(ka)]\right\}^{-1} \quad (36)$$

By assuming $k_0a \gg 1$ (Section VII), the asymptotic Bessel function expansions can be used for $m<$(argument). All other terms with $m\gtrsim$(argument) will be neglected since the Q of these modes is large (Section II). Making these approximations [19],

$$F_m \approx \frac{\frac{1}{i}\sqrt{\frac{\pi k_0a}{2}}\,e^{ik(r_1-a)}e^{-i(k_0r_1-m\pi/2-\pi/4)}}{1+\frac{1}{2}\left(\frac{k}{k_0}-1\right)(e^{2ik(r_1-a)}+1)}. \quad (37)$$

The average radiated power density is given by

$$p = \frac{E_0^2}{Z_{0\pi}}\sum_{m=-\infty}^{+\infty}|F_m|^2 \quad (38)$$

where

$$|F_m|^2 \approx \frac{\frac{\pi k_0a}{2}\,e^{-2\alpha k_0(r_1-a)}}{1\left|+\frac{1}{2}\left(\frac{k}{k_0}-1\right)(e^{2ik(r_1-a)}+1)\right|^2} \quad (39)$$

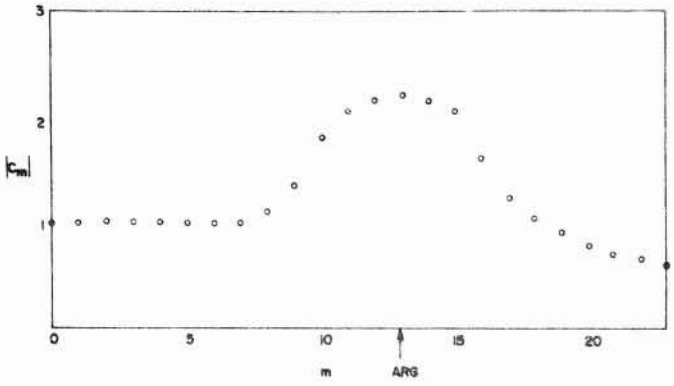

Fig. 10. Fourier coefficients for an argument of 13, m running from 0 to 25.

which is independent of m, so that

$$P \approx \frac{E_0^2}{Z_0} \frac{\frac{k_0 a}{2} e^{-2ak_0(r_1 - a)}}{\left|1 + \frac{1}{2}\left(\frac{k}{k_0} - 1\right)(e^{2ik(r_1 - a)} + 1)\right|^2} \sum_{m=-k_0 a}^{+k_0 a} (1) \quad (40)$$

and

$$P \approx \frac{E_0^2}{Z_0} \frac{(k_0 a)^2 e^{-2ak_0(r_1 - a)}}{\left|1 + \frac{1}{2}\left(\frac{k}{k_0} - 1\right)(e^{2ik(r_1 - a)} + 1)\right|^2}. \quad (41)$$

An actual set of coefficients has been computed for the sum in (40) (Fig. 10) for comparison with the approximate values of unity for each term.

Acknowledgment

The author would like to express his appreciation to Dr. R. Hermann and J. Thoenes of the University of Alabama Research Institute for helpful discussions of the sheath properties. An IBM 360/50 computer in Huntsville, Ala., was used to calculate data for several graphs included in the paper.

References

[1] T. M. Smith and K. E. Golden, "Radiation patterns from a slotted cylinder surrounded by a plasma sheath," *IEEE Trans. on Antennas and Propagation*, vol. AP-13, pp. 775–780, September 1965.

[2] R. E. Collin and S. Rothschild, "Evaluation of antenna Q," *IEEE Trans. on Antennas and Propagation*, vol. AP-12, pp. 23–27, January 1964.

[3] H. C. Kyle, *Manned Spacecraft: Engineering Design and Operation*. P. E. Purser et al. Eds. New York: Fairchild, 1964, ch. 28.

[4] F. J. Tischer, *Basic Theory of Space Communications*. Princeton, N. Y.: Van Nostrand, 1965, ch. 6.

[5] G. N. Krassner and J. V. Michaels, *Introduction to Space Communication Systems*. New York: McGraw-Hill, 1964, pp. 144–145.

[6] R. Lehnert and B. Rosenbaum, "Plasma effects on Apollo re-entry communications," Goddard Space Flight Center, Rep. X-513-64-8, January 1964 (superseded by NASA Tech. Note D-2732).

[7] R. Hermann and J. Yalamanchili, "Hypersonic flow with non-equilibrium disassociation around blunt bodies in flow facilities and in free flight," Yearbook 1965 of Wissensch. Ges. f. Luft- und Raumfahrt, Braunschweig, 1965.

[8] P. W. Huber and T. E. Sims, "The entry communications problem," *J. Astronautics and Aeronautics*, pp. 30–40, October 1964.

[9] R. Hermann, "Hypersonic non-equilibrium flow and its thermodynamic relations," University of Alabama Research Inst., Hunts-Bedford, Mass., Rept. 65-51, January 1965.

[10] H. R. Griem, *Plasma Spectroscopy*. New York: McGraw-Hill, 1964, ch. 6.

[11] W. R. Garrett and F. H. Mitchell, Jr., "Microwave propagation through plasma media," University of Alabama Research Inst., Huntsville, Rep. 34, January 1966.

[12] R. J. Papa, "Plane-wave propagation in a nonlinear, inhomogeneous, time-dependent plasma medium," AF Cambridge Research Labs., Bedford, Mass., Rept. 65-51, January 1965.

[13] A. T. Villeneuve, "Propagation of electromagnetic waves through inhomogeneous slabs," *IEEE Trans. on Antennas and Propagation*, vol. AP-13, pp. 926–933, November 1965.

[14] R. J. Papa, "The nonlinear interaction of an electromagnetic wave with a time-dependent plasma medium," *Canadian J. Phys.*, vol. 43, pp. 38–55, January 1965.

[15] J. R. Wait, "Radiation from a spherical aperture antenna immersed in a compressible plasma," *IEEE Trans. on Antennas and Propagation*, vol. AP-14, pp. 360–368, May 1966.

[16] S. R. Seshadri, "Radiation from an electromagnetic source in a half-space of compressible plasma-surface waves," *IEEE Trans. on Antennas and Propagation*, vol. AP-12, pp. 340–348, May 1964.

[17] H. Hodara and G. I. Cohn, "Radiation from a gyro-plasma coated magnetic line source," *IRE Trans. on Antennas and Propagation*, vol. AP-10, pp. 581–593, September 1962.

[18] C. T. Swift, "Radiation from slotted-cylinder antennas in a re-entry plasma environment," NASA Tech. Note D-2187, p. 33, February 1964.

[19] M. Abramowitz et al., *Handbook of Mathematical Functions*. U. S. Dept. of Commerce, Appl. Math. Series 55, p. 364, June 1964.

[20] F. H. Mitchell, Jr., "Radiation through plasma adjoining a conducting surface," *IEEE Trans. on Antennas and Propagation (Correspondence)*, vol. AP-13, pp. 468–469, May 1965.

[21] T. R. McPherron, P. J. Anderson, and A. F. Ruehe, "Study and experimentation on modulation degradation by ionized flow fields," McDonnell Aircraft Corp., St. Louis, Mo., Tech. Rept. AFAL-TR-65-46, pp. 26–36, February 1965.

[22] ——, "Saturn antenna systems SA-5," vol. 1–3, Astrionics Div., NASA, Marshall Space Flight Center, Huntsville, Ala., 1963.

[23] F. J. Tischer, "Communication blackout at re-entry," University of Alabama Research Inst., Huntsville, Rept. 6, September 1963.

[24] W. M. McCabe and C. F. Stolwyk, "Electromagnetic propagation through shock ionized air surrounding glide re-entry spacecraft," *IRE Trans. on Space Electronics and Telemetry*, vol. SET-8, pp. 257–266, December 1962.

[25] R. Hermann, "Hypersonic aerodynamic problems at re-entry of space vehicles," University of Alabama Research Inst., Huntsville, Rept. 29, November 1965.

Federal Systems Division, Space Systems Center, Huntsville, Alabama